Influence of Cobalt Doping on the Photogenerated Holes in ZnO Nanoparticles

Zahraa Jradi, Dara Marin, Andréa Campos, Martin O'byrne, Olivier Margeat, Sylvain Bertaina, Adrien Savoyant

physica status solidi rrl
www.pss-rapid.com

Influence of Cobalt Doping on the Photogenerated Holes in ZnO Nanoparticles

*Zahraa Jradi, Dara Marin, Andréa Campos, Martin O'Byrne, Olivier Margeat, Sylvain Bertaina, and Adrien Savoyant**

The efficient cobalt doping of zinc oxide nanoparticles grown by chemical method, with Co^{2+} substituting the Zn^{2+} cations, is proved by electron spin resonance spectroscopy for cobalt concentration from 0.01% to 1.00%. The gradual killing of the usual core-defect signal ($g \approx 1.96$) as the Co concentration is increased prevents its ionization by optical excitation from X^0 to X^-, thus inhibiting the corresponding hole releasing. Consequently, the $^{\bullet}CH_3$ methyl radical is no longer generated on the nanoparticles surface by the photo-Kolbe reaction $h^+ + CH_3COO^- \rightarrow {}^{\bullet}CH_3 + CO_2$. It is thus confirmed that the hole involved in the dissociation of surface acetate actually comes from the optically excited core-defect $g = 1.96$, and that the number of these defects can be tuned by some very small amount of cobalt impurities.

1. Introduction

One of the most striking and useful features of zinc oxide (ZnO) crystals is their ability to generate charge carriers when subjected to optical excitation in the visible or near-UV range. The main illustration of this is the generation of stable exciton even at room temperature with binding energy of 60 meV below the conduction band minimum.[1] This fact is at the heart of many applications of ZnO materials, especially in the fields of optoelectronics and photocatalysts.[2] Apart from the excitonic phenomena occurring even in perfect material (intrinsic property), some point defects can be ionized by optical excitation with an energy notably below the bandgap (between 3.1 and 3.4 eV), capturing or releasing charge carriers. This point-defect ionization can also be seen as a bound exciton in which one of the photogenerated carrier is trapped at the defect site, the other remaining more or less free to move within the crystal before it recombines. The type (electron or hole), the quantity, and the lifetime of these photogenerated carriers depend on the presence and type of point defects, on the excitation energy, and on the temperature. Moreover, in nanosized materials such as nanoparticles (NPs), size and postgrowth treatment also play a role in this charge-carrier photogeneration. This explains the great interest for ZnO NPs with dimensions between 10 and 50 nm in diameter for which carriers can reach the surface and can possibly interact with surface species.[3]

While most of the applications of such photogenerated carriers reaching the NPs surface is to make them react with some chemically adsorbed species continuously refreshed (photocatalyst), the possibility exists to induce a surface reaction with paramagnetic species in the final state, both products and reactants remaining on the surface (no species flow). For example, in ZnO NPs, a laser excitation of 405 nm wavelength applied at low temperature (<120 K) generates a surface methyl radical,[4,5] detected by electron paramagnetic resonance (EPR). This has been interpreted as a kind of photo-Kolbe reaction[6,7] in which the photogenerated hole is released by a point-defect ionization (rather than from an intrinsic exciton), and the methyl radical originates from the resulting dissociation of surface-adsorbed zinc acetate. In this example, the involved point defect is a relatively deep acceptor (0.4 eV below the conduction band), most probably a neutral zinc vacancy (V^0_{Zn}) or a complex of it (e.g., the stoichiometric defect $(V_{zn}–Zn_i)^0$). This so-called core-defect resonating at $g \simeq 1.96$[8–10] is denoted by *X* in the following. The optically generated quasistable surface magnetic state (a methyl radical $^{\bullet}CH_3$ in this case) is then susceptible to be manipulated by various pulse-EPR sequences, paving the way to monitorable spin embedded in nanosized system, with potential application in the field of quantum sensing or computing.[5] It is then clear that the conditions for inhibiting or enhancing the holes generation are of high interest.

Z. Jradi, D. Marin, S. Bertaina, A. Savoyant
Aix Marseille University
CNRS
IM2NP
Marseille, France
E-mail: adrien.savoyant@im2np.fr

A. Campos
CNRS
Centrale Marseille
FSCM (FR1739)
CP2M
Aix Marseille University
13397 Marseille, France

M. O'Byrne, O. Margeat
Aix Marseille University
CNRS
CINAM
Marseille, France

The ORCID identification number(s) for the author(s) of this article can be found under https://doi.org/10.1002/pssr.202300341.

DOI: 10.1002/pssr.202300341

2. Results and Discussion

In this work, it is demonstrated that the number of photogenerated holes by the core defects changing from its initial state X^0 to X^- can be controlled by introducing very small amount of substitutional cobalt impurities within the ZnO matrix. The basic process under consideration involved 1) one bulk reaction activated by the optical quantum $h\nu = 3$ eV, 2) the migration of the photogenerated hole from bulk to surface, and 3) finally the dissociation of the adsorbed acetate molecule.

$$X^0 \rightarrow X^- + h^+ \,(\text{bulk}) \tag{1}$$

$$h^+ \,(\text{bulk}) \rightarrow h^+ \,(\text{surf.}) \tag{2}$$

$$h^+ + CH_3COO^- \rightarrow {}^{\bullet}CH_3 + CO_2 \,(\text{surf.}) \tag{3}$$

While the initial states of the reactions (1) and (3) are both nonmagnetic (no EPR signal), their final states contain paramagnetic species X^- ($g \simeq 1.960$, one EPR line) and ${}^{\bullet}CH_3$ ($g \simeq 2.003$, four EPR lines), respectively, so that the relative quantity of each can be followed by following the EPR intensities.

According to the aboveproposed mechanism, the final generation of methyl radical ${}^{\bullet}CH_3$ is subjected to three main limitations: 1) the presence of the initial neutral defect X^0 releasing the hole under optical excitation; 2) the possibility for the hole to reach the surface before recombination; and 3) the presence of surface-adsorbed negatively charged acetate CH_3COO^- capturing the hole.

In the following, it is shown that postgrowth annealing is related to limitation (3) by removing all organic species from the surface and that the cobalt doping is related to limitation (1) by suppressing the neutral defect X^0 and, consequently, the number of photogenerated holes. In addition, it can be noted that limitation (2) implies to work at sufficiently low temperature (<120 K) for avoiding the hole recombination with the ubiquitous n-type carriers of ZnO (from hydrogen impurities or oxygen vacancies).

Based on the fact that cobalt doping of ZnO nanostructures is known to suppress the ionized core-defect X^- signal ($g \simeq 1.96$),[11] the present work aims to verify that this doping also results in the blockage of the methyl generation, by preventing hole releasing involved in the reactions (1)–(3). Similar competing effects have also been observed for the Mn-doped ZnO NPs.[12] In order to investigate both the effect of annealing and of the cobalt doping, four samples have been prepared with Co molar concentrations of 0.00, 0.01, 0.10, and 1.00% by introducing the appropriate amount of cobalt acetate with respect to zinc acetate in the wet chemical growth method described in ref. [5] These nominal concentrations do not correspond to the substitutional cobalt content effectively entering the ZnO matrix, which is much lesser, but are supposed to scale with. A part of each of these as-grown dried powders has been heated at 500 °C for 5 min in order to obtain the annealed samples.

The structural and morphological properties of the NPs powders under study have been investigated by transmission electron microscopy (TEM) and scanning electron microscopy (SEM). Representative results of these measurement are shown in **Figure 1** for both the as-grown and annealed 0.1% cobalt samples. The first point is that cobalt doping under 1% does not notably change the morphological and structural quality

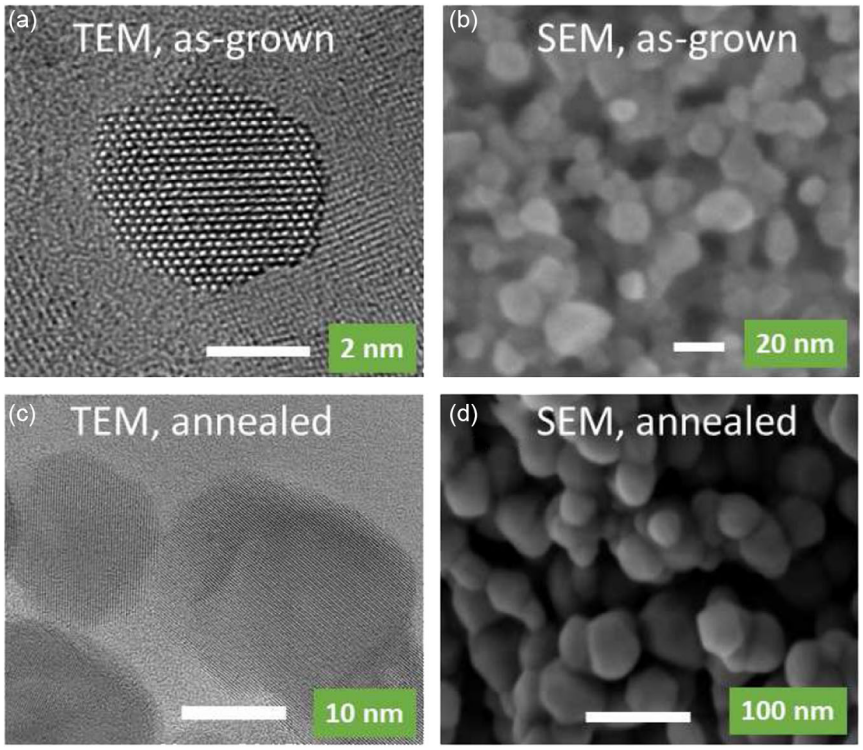

Figure 1. a,b) TEM and SEM imaging of as-grown ZnO NPs with 0.1%Co. c,d) The same for annealed ZnO NPs with 0.1% Co.

of the NPs. On the contrary, the sample annealing results in a NP size increase by a factor of ≈ 3 (from 15 to 50 nm of mean diameter), as shown by the SEM imaging of the present and previous studies.[13] TEM measurements (performed on the smallest of the NPs found) display a clear wurtzite (hexagonal) structure of the faceted NPs, irrespective of the cobalt content.

The structural crystal quality is also confirmed by X-ray diffraction (XRD) measurements (**Figure 2**, left panels), showing the usual (*h, k, l*) planes of the wurtzite structure (JCPDS Card No: 01-079-2205). The crystallinity, understood as the spatial coherence of the material, is again found to be almost unsensitive to the cobalt doping, but is notably increased after annealing of the samples, as shown by the peak narrowing, consistently with a NP size increase.

Aside of these structural and morphological analyses, the Fourier-transform infrared spectroscopy (FTIR) experiment provides information on the common organic molecules present in the different samples (Figure 2, right panels). To this purpose, the ZnO NP solution has been spin coated onto an IR transparent Si substrate. The main information obtained is that in all as-grown samples, vibration modes of organic bounds OH, COO^-, and CH are detected,[14] consistent with a previous study proving the presence of acetate $CH_3CH_3OO^-$ at the surface of the ZnO NPs, originating from the zinc acetate precursor. As the cobalt content is increased, many additional vibration modes appear in the region 1000–2000 cm^{-1}, which disappear upon annealing. This can be attributed to some residual complexes of surface-adsorbed cobalt acetate, evaporated by heating. In addition, an intriguing positive peak at around 1100 cm^{-1} is detected (very intense in the 0% samples), which may be attributed to an artefact of the measurement or some possible emission phenomena briefly mentioned in Conclusion.

Next, the efficiency of substitutional cobalt doping within the ZnO matrix is investigated by EPR, performed on the annealed samples in order to avoid the parasite signals from the above-mentioned residual surface-adsorbed cobalt-acetate. The results obtained in the dark (no optical excitation) are displayed in **Figure 3**, showing a clear CO^{2+} powder spectrum in easy-plane axial symmetry.[15–18] The different spectra have been normalized as follows: first, starting from the 1% cobalt signal as reference, the 0.1% cobalt signal is scaled to be 10 times weaker. Then, the surface defect line ($g = 2.003$) being not so different in these two scaled spectra, it is assumed that this line intensity

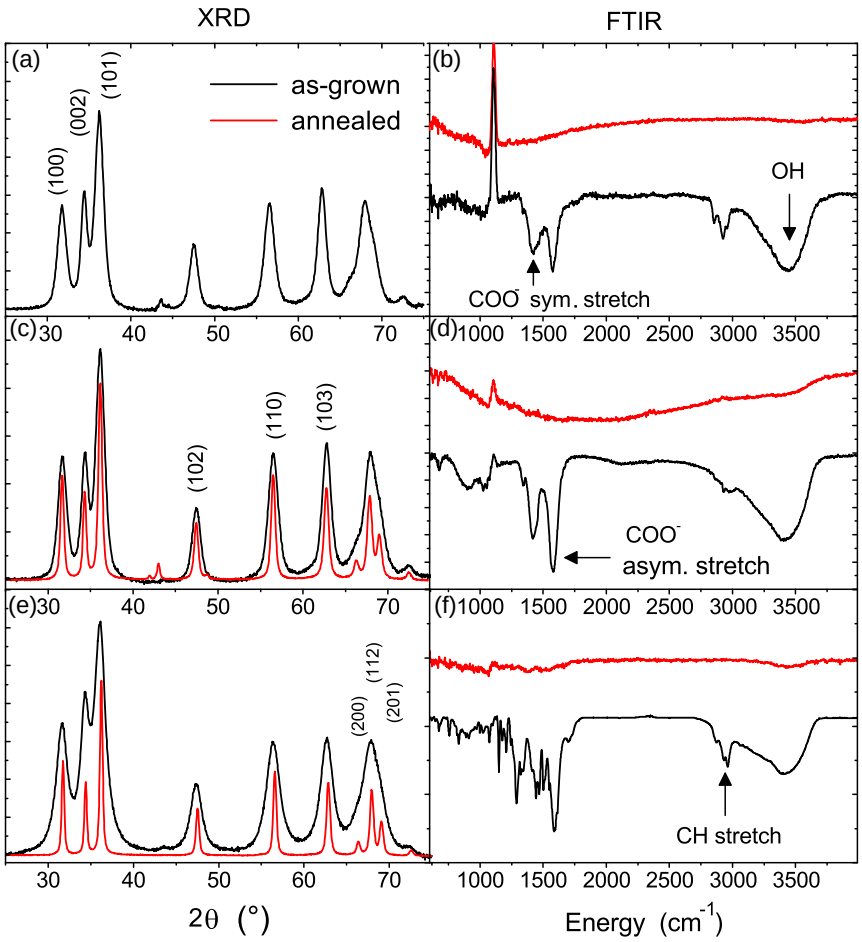

Figure 2. XRD (left column) and FTIR (right column) results on ZnO NPs samples. a,b) 0.00% Co. c) 0.01% Co. d) 0.10% Co. e,f) 1.00% Co. For all panels, black line corresponds to as-grown samples and red line to the annealed samples.

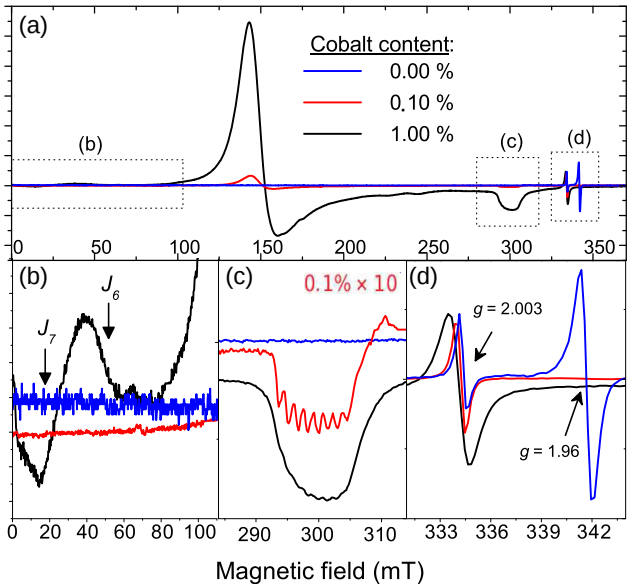

Figure 3. EPR spectra of annealed samples in the dark for various cobalt concentrations. a) Full-range spectra, b) low-field lines, c) hyperfine structure of $B\|c$ orientation, and d) surface- ($g = 2.003$) and core-defect ($g = 1.960$) lines.

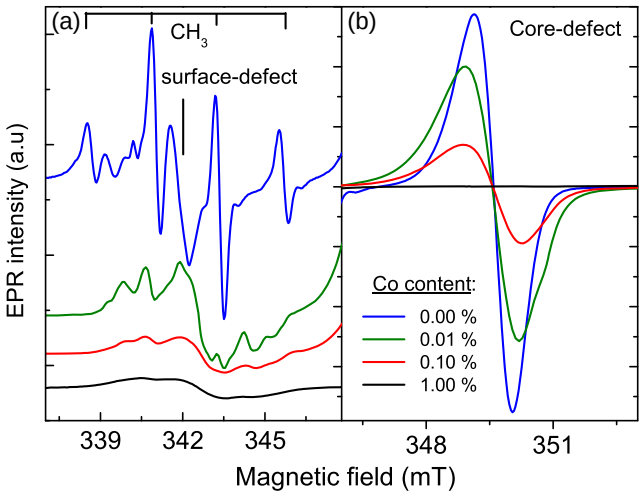

Figure 4. Light-induced EPR signals recorded on the as-grown samples at 15 K for various cobalt concentrations. a) Zoom on the radicals and surface-defects region $g \approx 2$. b) The core-defect region ($g \approx 1.96$.).

is almost insensitive to the cobalt content. The 0% cobalt sample spectrum is thus scaled so as to have an almost identical surface-defect intensity as the 0.1% cobalt sample.

From these scaled spectra, much consistent information is obtained. In the low-field region, the two near-zero-field lines are observed only in the most-doped sample (1%), corresponding to Co–Co pairs J_6 and J_7 (Figure 3b).[18,19] Around 300 mT, the $B\|c$ orientation of the powder spectrum shows trace of the hyperfine splitting for the 1% sample, better resolved in the 0.1% sample (10 times magnified) because of weaker dipolar broadening (Figure 3c). The 8 lines spaced by 1.6 mT corresponds to those of a substitutional Co^{2+} ion in the ZnO matrix and its resolution point to a high crystallinity of the NPs. In the region 330–350 mT (Figure 3d), surface-defect signal ($g = 2.003$)[8,9] is visible in all samples, while the core-defect one ($g = 1.960$) is visible only in the undoped samples. This is consistent with the previous finding that, first, annealing removes the surface-adsorbed acetate CH_3COO^-, thus oxidizing the core-defect X^0 to X^- in the absence of illumination[5] and, second, that even a small amount of cobalt impurities destroy the core-defect signal.[11]

The final point of this work is the following of the core-defect and the methyl radical signals intensity as a function of the cobalt concentration in the as-grown samples and under 405 nm wavelength illumination. The resulting spectra are shown in **Figure 4**. In the extreme case of pure ZnO NPs (0% cobalt), the photogenerated signal is clearly dominated by the four-line structure of methyl radical around $g = 2.003$ and by an intense core defect ($g = 1.960$). The surface-defect line is also visible at $g = 2.003$ as well as other weaker lines between those of methyl, likely to arise from other types of photogenerated radicals. In the opposite case (1% cobalt), the core-defect signal is no longer generated at all, and so is the same for the methyl radical signal. In the intermediate doping cases (0.1% and 0.01%), the core-defect and the methyl signals display intermediate EPR intensities, progressively disappearing together as the Co content is increased.

3. Conclusion

From the presented results, it is possible to conclude that, as observed in other ZnO nanostructures, a very low amount of cobalt destroys the usual core-defect signal photogenerated in as-grown samples or present in the dark in the annealed sample. In the as-grown sample, this number of core defects is directly related to the $^{\bullet}CH_3$ radical generation via the three-step mechanism presented in Equation (1) to (3), the last one being a kind of photo-Kolbe reaction involving the photogenerated hole. Consequently, the amount of these photogenerated holes can be controlled by the temperature (for avoiding recombination with electrons) but also by cobalt incorporation in the ZnO NPs with the results of inhibiting the core-defect ionization at the origin of the hole releasing. This finding is susceptible to be related to the positive peak observed in the FTIR spectra, possibly arising from hole radiative recombination, which progressively disappears as the Co content is increased. These results give insight into the defect engineering related to photocatalysts and the p-type carrier generation in ZnO NPs.

Acknowledgements

This work was supported by Agence Nationale de la Recherche (ANR project "SPIMAN", ANR-21-CE09-0027-01). Financial support from the IR INFRANALYTICS FR2054 for conducting the research is gratefully acknowledged.

Conflict of Interest

The authors declare no conflict of interest.

Data Availability Statement

The data that support the findings of this study are available from the corresponding author upon reasonable request.

Keywords

cobalt doping, holes, nanoparticles, optical excitations, point defects, ZnO

Received: August 29, 2023
Revised: October 16, 2023
Published online:

[1] Ü. Özgür, Y. I. Alivov, C. Liu, A. Teke, M. A. Reshchikov, S. Doğan, V. Avrutin, S.-J. Cho, H. Morkoç, *J. Appl. Phys.* **2005**, *98*, 041301.
[2] C. B. Ong, L. Y. Ng, A. W. Mohammad, *Renewable Sustainable Energy Rev.* **2018**, *81*, 536.
[3] J. Haque, M. Bellah, R. Hassan, S. Rahman, *Nano Express* **2020**, *1*, 010007.
[4] A. Savoyant, C. Sebastiao, O. Margeat, *Phys. Status Solidi RRL* **2020**, *14*, 2000176.
[5] D. Marin, G. Gerbaud, O. Margeat, F. Ziarelli, F. Ferrer, O. Ouari, A. Campos, S. Bertaina, A. Savoyant, *J. Chem. Phys.* **2023**, *158*, 184704.
[6] M. Schmitt, S. Kuhn, M. Wotocek, R. Hempelmann, *Z. Phys. Chem.* **2011**, *225*, 297.
[7] M. Schmitt, *Macromol. Chem. Phys.* **2012**, *213*, 1953.
[8] H. Kaftelen, K. Ocakoglu, R. Thomann, S. Tu, S. Weber, E. Erdem, *Phys. Rev. B* **2012**, *86*, 014113.
[9] E. Erdem, *J. Alloys Compd.* **2014**, *605*, 34.
[10] S. Repp, S. Weber, E. Erdem, *J. Phys. Chem. C* **2016**, *120*, 25124.
[11] A. Savoyant, H. Alnoor, O. Pilone, O. Nur, M. Willander, *Nanotechnology* **2017**, *28*, 285705.
[12] T. Ruf, S. Repp, J. Urban, R. Thomann, E. Erdem, *J. Nanopart. Res.* **2016**, *18*, 109.
[13] A. K. Diallo, M. Gaceur, N. Berton, I. Shupyk, G. Poize, S. Nénon, O. Margeat, C. Videlot-Ackermann, J. Ackermann, *Int. J. Nanotechnol.* **2014**, *11*, 819.
[14] T. Thangeeswari, A. T. George, A. Arun Kumar, *Indian J. Sci. Technol.* **2016**, *9*, 1.
[15] J. Chess, G. Alanko, D. A. Tenne, C. B. Hanna, A. Punnoose, *J. Appl. Phys.* **2013**, *113*, 17C302.
[16] F. Acosta-Humànez, R. Cogollo Pitalùa, O. Almanza, *J. Magn. Magn. Mater.* **2013**, *329*, 39.
[17] T. J. Castro, P. A. M. Rodrigues, A. C. Oliveira, F. Nakagomi, J. Mantilla, J. A. H. Coaquira, A. Franco Jùnior, H. V. S. Pessoni, P. C. Morais, S. W. da Silva, *J. Appl. Phys.* **2017**, *121*, 013904.
[18] D. Marin, S. K. Tiwari, S. Bertaina, A. Savoyant, *Phys. Rev. B* **2022**, *105*, 035424.
[19] A. Savoyant, F. Giovannelli, F. Delorme, A. Stepanov, *Semicond. Sci. Technol.* **2015**, *30*, 075004.